JOURNAL OF GEOPHYSICAL RESEARCH, VOL. 111, B12306, doi:10.1029/2005JB004059, 2006



# A new 1649–1884 catalog of destructive earthquakes near Tokyo and implications for the long-term seismic process

Elliot D. Grunewald[1,2] and Ross S. Stein[1]

Received 19 September 2005; revised 25 July 2006; accepted 28 August 2006; published 20 December 2006.

[1] In order to assess the long-term character of seismicity near Tokyo, we construct an intensity-based catalog of damaging earthquakes that struck the greater Tokyo area between 1649 and 1884. Models for 15 historical earthquakes are developed using calibrated intensity attenuation relations that quantitatively convey uncertainties in event location and magnitude, as well as their covariance. The historical catalog is most likely complete for earthquakes $M \geq 6.7$; the largest earthquake in the catalog is the 1703 $M \sim 8.2$ Genroku event. Seismicity rates from 80 years of instrumental records, which include the 1923 $M = 7.9$ Kanto shock, as well as interevent times estimated from the past ~7000 years of paleoseismic data, are combined with the historical catalog to define a frequency-magnitude distribution for $4.5 \leq M \leq 8.2$, which is well described by a truncated Gutenberg-Richter relation with a $b$ value of 0.96 and a maximum magnitude of 8.4. Large uncertainties associated with the intensity-based catalog are propagated by a Monte Carlo simulation to estimations of the scalar moment rate. The resulting best estimate of moment rate during 1649–2003 is $1.35 \times 10^{26}$ dyn cm yr$^{-1}$ with considerable uncertainty at the 1$\sigma$ level: $(-0.11, + 0.20) \times 10^{26}$ dyn cm yr$^{-1}$. Comparison with geodetic models of the interseismic deformation indicates that the geodetic moment accumulation and likely moment release rate are roughly balanced over the catalog period. This balance suggests that the extended catalog is representative of long-term seismic processes near Tokyo and so can be used to assess earthquake probabilities. The resulting Poisson (or time-averaged) 30-year probability for $M \geq 7.9$ earthquakes is 7–11%.

**Citation:** Grunewald, E. D., and R. S. Stein (2006), A new 1649–1884 catalog of destructive earthquakes near Tokyo and implications for the long-term seismic process, *J. Geophys. Res.*, *111*, B12306, doi:10.1029/2005JB004059.

## 1. Introduction

[2] Tokyo is precariously situated near the junction of three tectonic plates and has been devastated by large earthquakes throughout its recorded history. In 1923, more than 140,000 people were killed in the great Kanto earthquake [*Imamura*, 1924; *Nyst et al.*, 2006]. In the ensuing years, the population of Tokyo has increased sixfold, making a deeper understanding of potentially destructive earthquakes especially urgent.

[3] One of the most powerful tools used in earthquake hazard analysis is the record of past earthquakes, which can be used to assess the possible size, rate, and distribution of future earthquakes. Instrumental records of seismicity in Japan are available for only the last century, a temporal snapshot far shorter than the interevent time of many large earthquakes. On the other hand, historical records of damage caused by earthquakes are remarkably well documented in Japan and extend back several centuries. These eyewitness damage descriptions have been interpreted as numerical intensity data to estimate locations and magnitudes of historical earthquakes in order to extend the earthquake record [*Utsu*, 1979, 1982a; *Usami*, 1994, 2003; *Bakun*, 2005].

[4] Intensity data provide meaningful constraints on the location and magnitude of historical earthquakes, but most previous studies do not adequately convey the significant uncertainties that are also associated with intensity modeling. In this study, we reanalyze historical earthquakes near Tokyo using a relatively new intensity modeling method developed by *Bakun and Wentworth* [1997] and *Bakun* [2005], which quantitatively conveys the uncertainties of the intensity data and methods. The resulting catalog can then be used in conjunction with Japan's instrumental catalog and rich paleoseismic record to understand the long-term character of seismicity near Tokyo.

## 2. Intensity Modeling Methods

[5] Most previous intensity modeling studies have used the isoseismal method to estimate earthquake location and magnitude. In these studies, isoseismal contours are drawn in the region affected by an earthquake to designate areas that observed similar intensities. Earthquake magnitude is then determined as a function of the area $A_x$, in which observed intensities are above a particular threshold $x$, and the epicenter is located in the center of the highest intensity

[1]U.S. Geological Survey, Menlo Park, California, USA.
[2]Now at Department of Geophysics, Stanford University, Stanford, California, USA.

observations. Following a massive synthesis of shaking and damage observations, *Usami* [2003] used the isoseismal method to build an extensive historical catalog of earthquakes in Japan. Despite this landmark accomplishment, the isoseismal method has significant weaknesses. Very often, the quantity and spatial distribution of intensity observations limit the precision with which $A_x$ and the location of the isoseismals can be determined. In addition, the isoseismal method utilizes only a subset of the intensity data and fails to provide a quantitative assessment of uncertainties implied by the entire data set.

[6] In this study, we use a different method to reanalyze selected earthquakes near Tokyo using intensity assignments from *Usami* [1994]. *Bakun and Wentworth* [1997] estimated location and moment magnitude of historical earthquakes in California using empirically derived intensity attenuation relationships. *Bakun* [2005] extended these methods to Japan and derived regional attenuation models based on the Japan Meteorological Agency (JMA) intensity and magnitude scale using local calibration events. *Bakun* [2005] developed two different attenuation models; one for shallow, crustal earthquakes (“Honshu model”) and one for lower-attenuation subduction earthquakes, including interplate and intraslab earthquakes (“subducting plate model”):

$$\text{Honshu} \qquad I_{PRED} = -1.89 + 1.42M_{JMA} - 0.00887\Delta_h - 1.66\log\Delta_h \tag{1}$$

$$\text{Subducting plate} \qquad I_{PRED} = -8.33 + 2.19M_{JMA} - 0.00550\Delta_h - 1.14\log\Delta_h, \tag{2}$$

where $I_{\mathrm{PRED}}$ is the predicted JMA intensity, $M_{\mathrm{JMA}}$ is the JMA magnitude, and $\Delta_h$ is the slant distance between the observation site and the hypocenter at depth.

[7] In order to estimate earthquake location and magnitude suggested by an entire set of intensity observations, we apply the same grid search algorithm used by *Bakun and Wentworth* [1997]. For a grid of trial epicenters we first calculate the trial intensity magnitude, $M_i$, for each intensity data pair, $M_i = f(I_{\mathrm{JMA},i}, \Delta_{h,i})$ where $f$ is either the Honshu or subducting plate equation; $I_{\mathrm{JMA},i}$ and $\Delta_{h,i}$ are the intensity observation and slant distance to the hypocenter at site $i$, respectively. Then, we calculate the mean of the trial intensity magnitudes, $M_{\mathrm{jma}}$ = mean($M_i$), and the root-mean-square statistical fit, RMS[$M_{\mathrm{jma}}$], for each trial epicenter,

$$\mathrm{RMS}[M_{\mathrm{jma}}] = \left[\mathrm{RMS}\left(M_{\mathrm{jma}} - M_i\right) - \mathrm{RMS}_0(M_{\mathrm{jma}} - M_i)\right], \tag{3}$$

where

$$\mathrm{RMS}\left(M_{\mathrm{jma}} - M_i\right) = \sqrt{\frac{\sum_i \left[W_i(M_{\mathrm{jma}} - M_i)\right]^2}{\sum_i W_i^2}} \tag{4}$$

and $\mathrm{RMS}_0$ ($M_{\mathrm{jma}} - M_i$) is the minimum RMS ($M_{\mathrm{jma}} - M_i$) in the search grid. $W_i$ is a distance weighting function from *Bakun* [2005] that forces higher RMS values for trial epicenters near conflicting intensity assignments. For locations where RMS is low, the trial epicenter achieves relatively consistent $M_i$ from the intensity observations.

**Table 1.** Conversions Used for *Usami* [1994] Intensity Records

| *Usami* [1994] Assignment | Numerical Value Used |
|---|---|
| *Damage Data* | |
| 4 | 4 |
| 4–5 | 4.5 |
| >4 | 4.5 |
| 5 | 5 |
| 5–(6) | 5.5 |
| 5–6 | 5.5 |
| >5 | 5.5 |
| 6 | 6 |
| 6–7 | 6.5 |
| 7 | 7 |
| *Felt Data* | |
| e | 3 |
| E | 4 |
| S | 5 |

[8] Contoured RMS[$M_{\mathrm{jma}}$] are related to percent confidence that the epicenter was located within a contour using Table 5b from *Bakun and Wentworth* [1997]. The location described by the lowest RMS value is termed the intensity center. For all possible locations, the most likely $M_{\mathrm{JMA}}$, hereafter $M$, is described by the local $M_{\mathrm{jma}}$, with a $1\sigma$ uncertainty of ±0.25 magnitude units [*Bakun*, 2005]. All earthquakes in this study are modeled using a grid search area of at least 100 km width.

## 3. Data

[9] The intensity data used in this study are derived from maps compiled by *Usami* [1994] in which JMA intensity observations were assigned to towns affected in historical earthquakes. Town names have been converted to global coordinates using modern maps. Ambiguous intensity assignments have also been converted to numerical values according to Table 1. Fifteen earthquakes that occurred between 1649 and 1884 and which have at least two damage-based intensity observations are modeled. Most data before 1649 are too sparse to be modeled with precision. Isoseismal contour maps for earthquakes since 1884 have been compiled by *Utsu* [1982a] and *Usami* [2003], but discrete intensity observations have not been published.

[10] The *Usami* [1994] observations (Table 1) include intensity data based on physical damage records as well as felt reports (personal accounts of shaking which can be approximately assigned to likely intensities). Felt data are much less reliable than damage-based intensity observations because they are influenced by extraneous factors, such as the sensitivity of the observers and the time of day when the earthquake occurred. In cases where felt data do not strongly conflict with intensity data, however, felt data can provide tighter constraints on earthquake location. For such earthquakes data sets, felt data are used to define location confidence contours, but only damage observations are used to calculate magnitude.

[11] A key element in the analysis is the selection of the attenuation relation for each earthquake, which requires judgment. The Honshu model assumes a depth of 5 km, and the subduction model uses a depth of 30 km, an approximate depth of the Philippine Sea Plate in the Kanto region [*Ishida*, 1992]. All earthquakes with a record of a tsunami are modeled with (2). Earthquakes with no tsunami

are modeled as subduction events, (2), if peak intensities are located near the coast; otherwise, (1) is used. For data sets in which intensity data are confined to a small area, we assume that these are relatively small events and use (1) in order to minimize magnitude exaggeration caused by depth assumptions.

## 4. Results

### 4.1. Intensity-Based Catalog

[12] Intensity centers for all 15 events analyzed here are shown in Figure 1a. Source parameters are listed in Table 2 with 1$\sigma$ magnitude uncertainty, and the location and magnitude models are shown in Appendix A. For most earthquakes, the best fit source parameters determined in this study are in relative agreement with those inferred by the *Usami* [2003] isoseismal study. In some cases, however, we infer a significantly different location or magnitude. Further, two earthquake in the catalog have insufficient intensity data to be adequately constrained by these methods. Examples of each of these cases are presented in sections 4.1.1–4.1.3 with a brief discussion and are shown in Figure 2.

#### 4.1.1. The 11 March 1853 Earthquake

[13] Most reports of damage for the 11 March 1853 earthquake come from near the Izu Peninsula (Figure 2a). *Usami* [2003] concluded $M$ = 6.7 ± 0.1 for this earthquake and placed the epicenter at the neck of the Izu Peninsula. Because the highest intensities are near the southern coast, this earthquake is analyzed using (2). The model, shown in Figure 2a, has well bounded location contours with an intensity center close to the Usami epicenter. The best estimate of magnitude, 7.0 (6.8–7.3), is also in agreement with the magnitude proposed by Usami.

#### 4.1.2. The 31 December 1703 Genroku Earthquake

[14] The 1703 Genroku earthquake was one of the most destructive shocks in Japan's recorded history. Much of the southern Kanto region experienced severe shaking, and a tsunami hit the Izu peninsula, Sagami Bay, and the east coast of the Boso Peninsula. The earthquake also caused uplift of bedrock as high as 6 m along the coast [*Shishikura*, 2003]. Numerous seismologists have created models for this earthquake using a combination of intensity data, tsunami runup height, and surface fault displacement [*Matsuda et al.*, 1978; *Usami*, 2003; *Shishikura and Toda*, 2003]. The most comprehensive study by *Shishikura and Toda* [2003] models the earthquake as $M_w$ = 8.2 (8.05–8.25) with slip on three main faults off the coast of the Boso Peninsula.

[15] Equation (2) is used to analyze the intensity data for this earthquake and the resulting model is shown in Figure 2b. The intensity center is located at the mouth of Sagami Bay and the estimated magnitude is 7.7 ± 0.25, much lower than the magnitude determined in the aforementioned studies.

[16] *Bakun* [2005] found his attenuation equations were accurate for even very large shocks, including one $M$ = 7.3 test earthquake and the great Kanto ($M$ ~ 7.9) shock. However, because the majority of the slip in the Genroku earthquake was located offshore, roughly half of the expected high-intensity observations are missing from the data set, so we may expect to underestimate the true magnitude. Intensity observations for the Genroku earthquake are very similar to observations from the 1923 Kanto

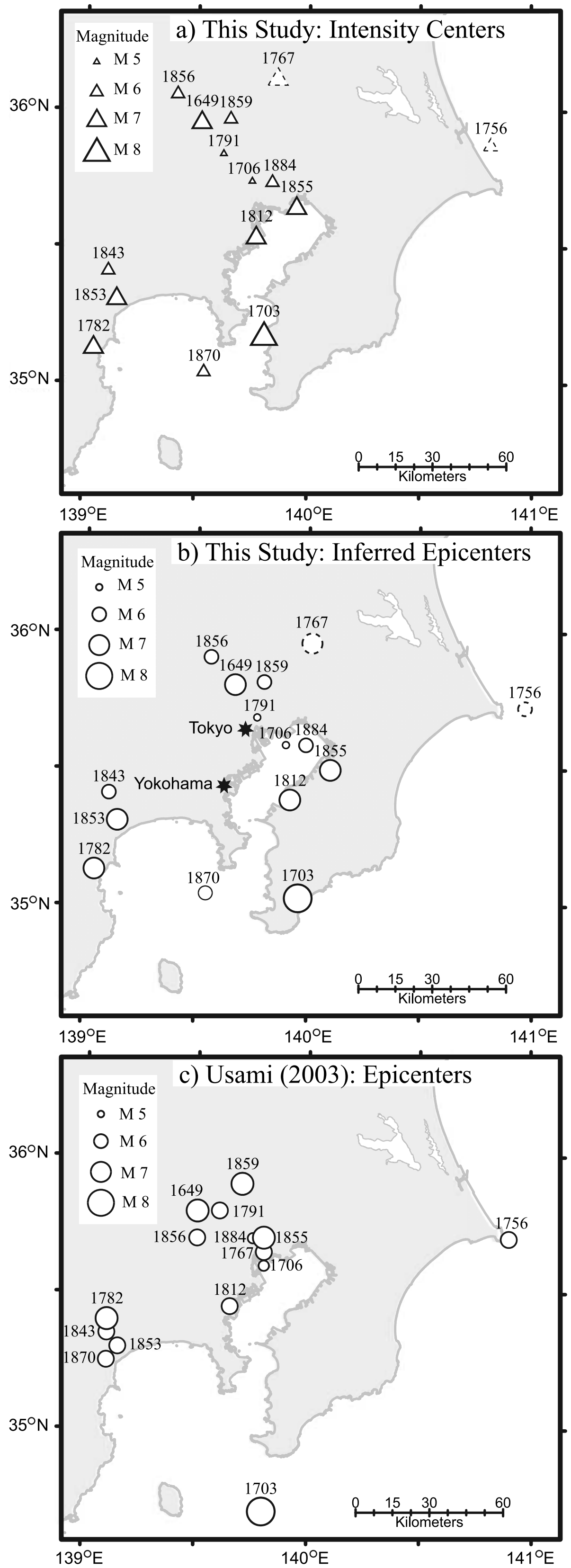


**Figure 1.** Three versions of the 1649–1884 intensity-based catalog. (a) Intensity centers determined in this study using *Bakun* [2005] intensity attenuation models (highly uncertain events dashed). (b) Epicenters inferred from intensity center-epicenter shift. (c) *Usami* [2003] epicenters.

**Table 2.** Model Parameters and Results for Earthquakes in the Historical Catalog

| | | | This Study | | | | | | *Usami* [2003] | | |
|---|---|---|---|---|---|---|---|---|---|---|---|
| | | | Intensity Center | | Inferred Epicenter | | | | | | |
| Date | Number of Observations | Attenuation Model[a] | Longitude | Latitude | Longitude | Latitude | JMA Magnitude | Uncertainty | Longitude | Latitude | JMA Magnitude |
| 07/30/1649 | 6 | Honshu-F | 139.75 | 35.92 | 139.50 | 35.76 | 7.0 | (6.7–7.5) | 139.5 | 35.8 | 7 |
| 12/31/1703 | 83 | Subduction-F | 139.81 | 35.18 | 139.66 | 35.03 | 8.2 | (8.1–8.3)[b] | 139.8 | 34.7 | 7.9–8.2 |
| 01/19/1706 | 6 | Honshu-F | 139.69 | 35.8 | 139.54 | 35.65 | 5.9 | (5.6–6.7) | 139.8 | 35.6 | 5.75 |
| 02/20/1756 | 6 | Subduction | 140.82 | 35.88 | 140.67 | 35.73 | 6.9 | (6.0–7.3)[c] | 140.9 | 35.7 | 5.5–6.0 |
| 10/22/1767 | 8 | Honshu | 139.86 | 36.12 | 139.71 | 35.97 | 7.0 | (6.0–7.2)[c] | 139.8 | 35.7 | 6 |
| 08/23/1782 | 48 | Subduction | 139.05 | 35.13 | 139.05 | 35.13 | 7.2 | (7.0–7.6) | 139.1 | 35.4 | 7 |
| 01/01/1791 | 15 | Honshu-F | 139.62 | 35.84 | 139.47 | 35.69 | 5.9 | (5.6–6.4) | 139.6 | 35.8 | 6.0–6.5 |
| 04/21/1812 | 23 | Subduction-F | 139.77 | 35.54 | 139.62 | 35.39 | 7.1 | (6.8–7.4) | 139.65 | 35.45 | 6.25 |
| 03/09/1843 | 20 | Subduction-F | 139.11 | 35.41 | 139.11 | 35.41 | 6.7 | (6.3–6.8) | 139.1 | 35.35 | 6.5 |
| 01/26/1853 | 59 | Subduction-F | 139.15 | 35.31 | 139.15 | 35.31 | 7.0 | (6.8–7.3) | 139.15 | 35.3 | 6.6–6.8 |
| 11/11/1855 | 191 | Subduction | 139.95 | 35.65 | 139.80 | 35.50 | 7.4 | (7.1–7.6) | 139.8 | 35.65 | 7.0–7.1 |
| 04/11/1856 | 33 | Honshu-F | 139.41 | 36.06 | 139.26 | 35.91 | 6.8 | (6.4–7.2) | 139.5 | 35.7 | 6.0–6.5 |
| 01/11/1859 | 6 | Honshu-F | 139.65 | 35.97 | 139.50 | 35.82 | 6.1 | (6.0–6.7) | 139.7 | 35.9 | 6.0–6.5 |
| 05/12/1870 | 8 | Subduction-F | 139.71 | 35.19 | 139.33 | 35.02 | 6.8 | (6.4–6.9) | 139.1 | 35.25 | 6 |
| 10/15/1884 | 6 | Subduction | 139.83 | 35.91 | 139.68 | 35.75 | 6.7 | (6.4–6.8) | 139.75 | 35.7 | NA |

[a]F, felt data used to constrain location.
[b]From *Shishikura and Toda* [2003].
[c]Highly uncertain.

earthquake, which ruptured only the nearshore portion of the 1703 source; collocated observations are only 0.26 $I_{JMA}$ units larger, on average, for the 1923 data set (S. Bozkurt et al., Forecasting probabilistic seismic shaking for greater Tokyo from 400 years of intensity observations, submitted to *Earthquake Spectra*, 2006). The similarity of these data sets suggests that the onshore intensity observations in 1703 are not sufficient to adequately estimate the slip offshore. Some degree of magnitude underestimation may also occur if the Genroku earthquake were accompanied by a significant component of slow slip. Slow earthquakes have been recorded east of the Boso Peninsula [*Ozawa et al.*, 2003], near the edge of the 1703 source, and any slow slip component would not be reflected in the intensity data set.

[17] Despite the considerable magnitude underestimation, the suggested location for the 1703 Genroku earthquake is reasonable because the gradient of onshore observations suggests an offshore source. The 67% confidence location contour for the intensity model closely outlines the faults inferred by *Shishikura and Toda* [2003]. Nonetheless, magnitudes estimated from tsunami runup heights and long-term deformation should more accurately represent the total moment release than the intensity-based model. Therefore in subsequent calculations of moment, magnitude estimates and uncertainty for this event are taken directly from *Shishikura and Toda* [2003] using a uniform probability distribution ($M$ = 8.05–8.25).

#### 4.1.3. The 22 October 1767 Earthquake

[18] On October 22, a strong earthquake was felt across a wide region between Edo (ancient Tokyo) and Sendai, in northeast Japan. Five aftershocks were felt the same day and one aftershock was felt the following day. Damage occurred

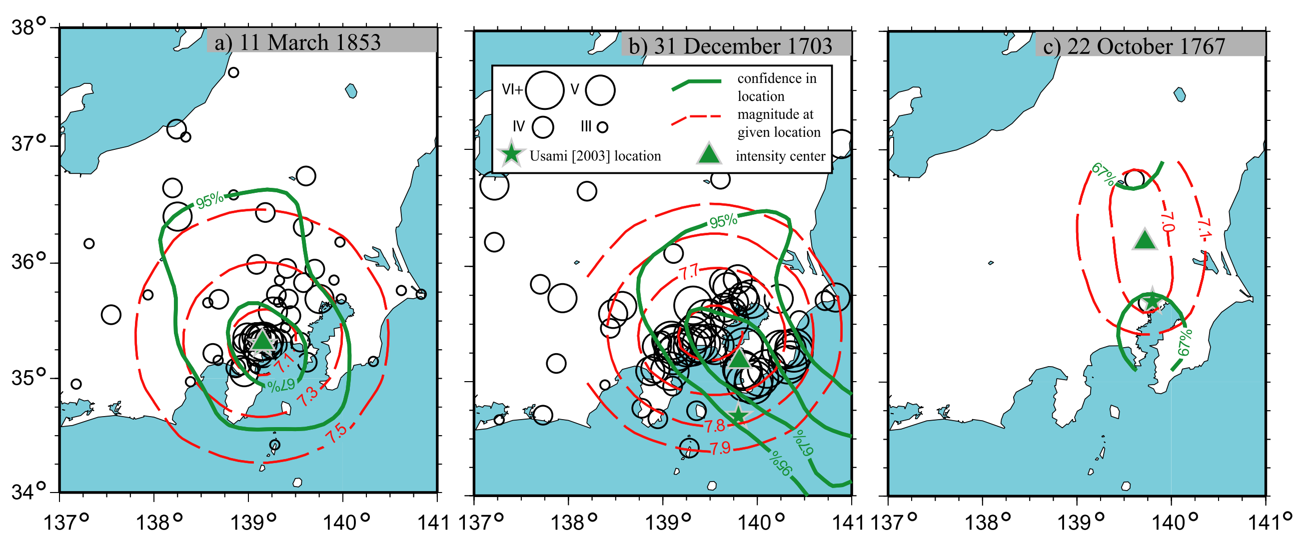


**Figure 2.** Example models for three catalog earthquakes. Dashed contours are $M_{jma}$ and solid contours are the 67% and 95% location confidence contours where shown. The triangle is the location of the intensity center and the star is the location of the *Usami* [2003] epicenter for (a) the 1853 event, (b) the 1703 Genroku shock, and (c) the 1767 event.

around Edo, and surface faulting was reported in a small town between Edo and Sendai [*Usami*, 2003]. The Honshu equation is used to model this event because intensities are observed well onshore and there is no record of tsunami.

[19] Only two damage-based intensity observations are available for this earthquake and felt reports are conflicting and unreliable. The intensity center location is not constrained by the data. This earthquake likely occurred somewhere between the two observations (Figure 2c) but the data is insufficient to determine a location with confidence. The two available data define magnitude contours that indicate $M$ = 7.0 over a broad region of possible epicenter locations around the data, including the location of the *Usami* [2003] epicenter.

[20] A similarly poor intensity data set is found for one other event, the 1756 earthquake near Chosi (see Appendix A). As in the previous case, the magnitude can be estimated ($M$ = 6.9–7.1) if the epicenter is assumed to be near the intensity observations as *Usami* [2003] concluded. Both of these earthquakes are exceptionally uncertain as a result of insufficient data, and their true uncertainties are underrepresented in these models.

### 4.2. Magnitude-Frequency Distribution

[21] In general, small earthquakes occur much more frequently than large ones. This relation is characterized by a famous equation of *Gutenberg and Richter* [1944]

$$\log n(M) = a - bM, \tag{5}$$

where $n(M)$ is the number of earthquakes larger than magnitude $M$. *Kagan* [1991] used a modified equation that includes a parameter, $M_{\max}$, for the maximum magnitude at which earthquakes can occur

$$\log n(M) = a - bM - k10^{1.5M}, \tag{6}$$

where $k = 10^{-1.5M\max}$. This is often referred to as a truncated Gutenberg-Richter distribution. If a catalog is consistent with a Gutenberg-Richter relationship for earthquakes above a certain magnitude, the catalog is considered complete for earthquakes above that threshold. So, we seek to establish the magnitude of completeness of the historical catalog.

[22] We determine the magnitude-frequency distribution for an extended catalog, which includes the 1649–1884 intensity-based catalog, an 1885–1922 catalog from *Utsu* [1982a], Japan's 1923–2003 instrumental catalog [*Japan Meteorological Agency (JMA)*, 2004] (Figure 3), and data from a 7000-year paleoseismic record. We assume that the intensity-based catalog is not complete for $M < 6.7$, since only three such events exist in this catalog, and determine the rate of earthquakes $4.5 \leq M < 6.7$ exclusively from the instrumental catalog. Instrumental $M < 6.7$ data from 1923 are not used since an anomalously high ratio of large to small aftershocks surround the 1923 great Kanto earthquake [*Hamada et al.*, 2001]. The rate of earthquakes $6.7 \leq M \leq 7.4$ is calculated using all available modern and intensity-based data from (1649–2003). Rates for the largest earthquakes, Taisho-type ($M \sim 7.9$, e.g., 1923 great Kanto earthquake) and Genroku-type ($M \sim 8.2$), are determined from paleoseismic records of 17 marine terraces, which

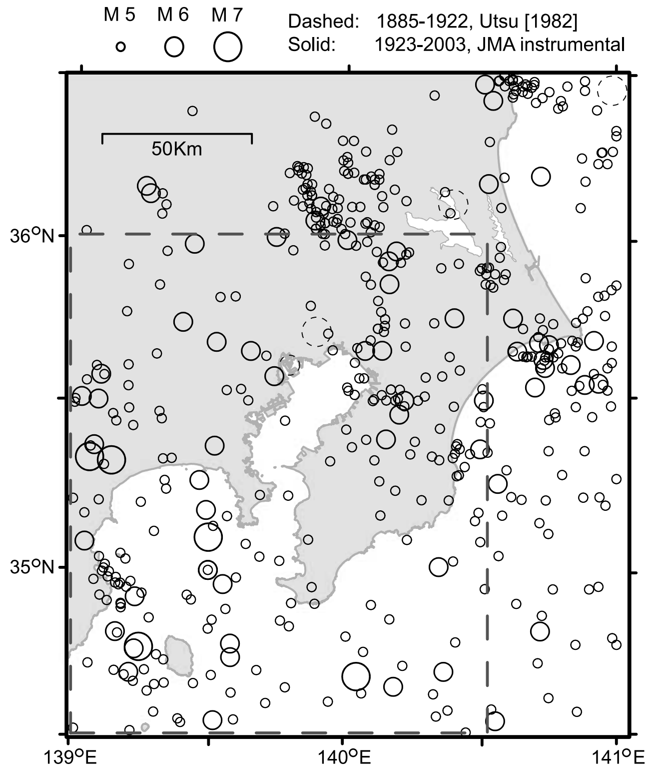


**Figure 3.** Earthquakes from other catalogs used in this study. Dashed circles are $M \geq 6.7$ from the 1885–1922 *Utsu* [1982a] catalog. Solid circles are $M \geq 5.0$ for the 1923–2003 catalog (JMA). The dashed box is the region of completeness for the intensity-based catalog.

were collected by *Matsuda et al.* [1978] and *Shishikura* [2003, also written correspondence, August 2004] and statistically analyzed by *Stein et al.* [2006]. The interevent time for $M_{JMA} \geq 7.9$ earthquakes is taken as 403 ± 66 years [*Stein et al.*, 2006]. For $M_{JMA} \geq 8.2$ Genroku-type events, the rate reflects the mean interevent time for the four widest Boso terraces, ~2200 years [*Shishikura*, 2003].

[23] We consider the magnitude-frequency distribution within two regions, a larger box that broadly surrounds Tokyo, and a smaller box covering only the area in which the intensity-based catalog is concentrated (Figure 3). Intensity centers for the 1767 and 1856 shocks lie just outside the northern border of the small box but are included in both because of their location uncertainties. The magnitude frequency distribution for the larger area (Figure 4a) shows a discontinuity between the trend of the $M < 6.7$ instrumental data (gray line) and the combined $M \geq 6.7$ data, implying that the intensity-based catalog may fail to capture some $M_{JMA} \geq 6.7$ shocks within this area, likely due to poor sensitivity in lightly populated areas and absence of offshore observations. Data from the smaller area (Figure 4b) conform more closely to a truncated Gutenberg-Richter relation over the full $4.5 \leq M \leq 8.2$ range, and so the catalog is more likely to be complete for $M \geq 6.7$ within this smaller area. A least squares regression of the *Kagan* [1991] equation determines a $b$ value of 0.96 and $M_{\max}$ = 8.40. This $b$ value is slightly higher than the regional value, $b$ = 0.85, determined from $1.5 \leq M \leq 5.6$ shocks for the period 1986–1996 [*Wyss and Wiemer*, 1997].

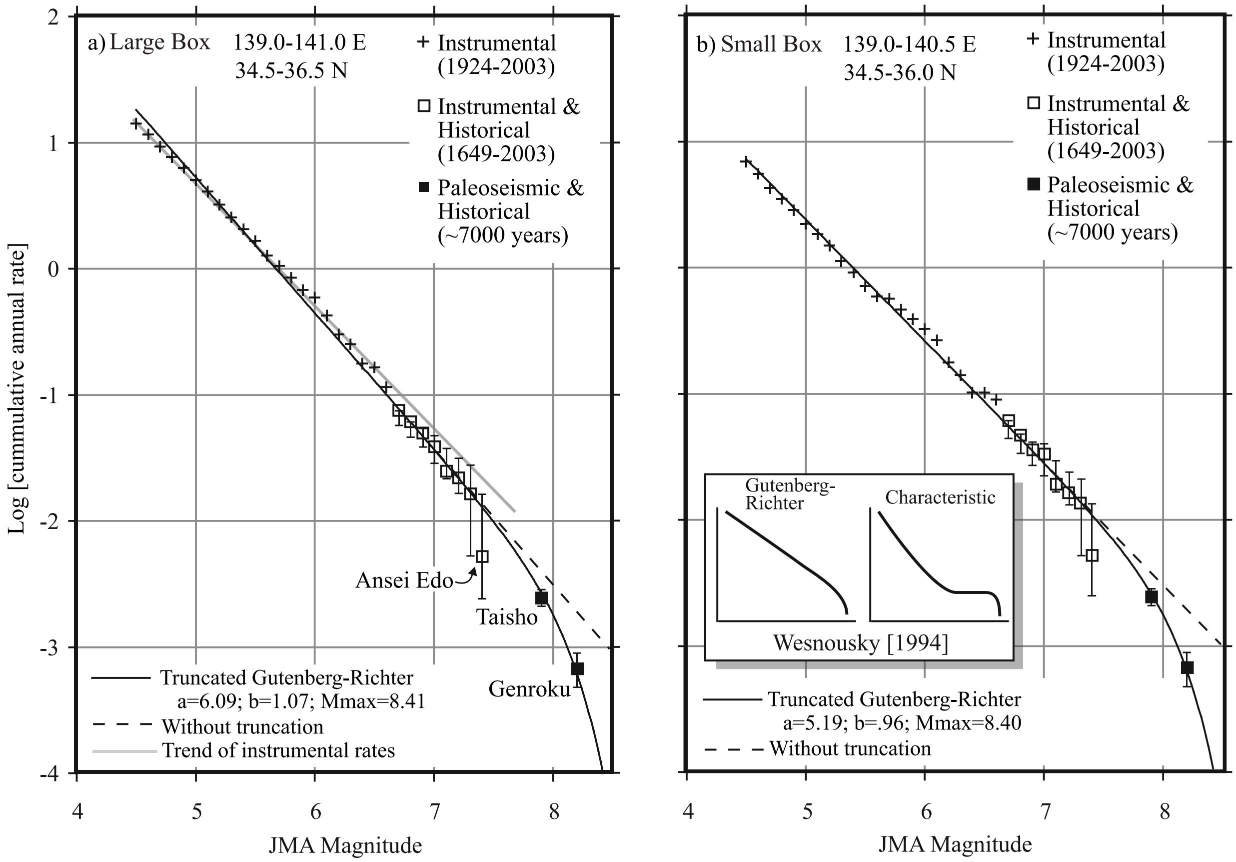


**Figure 4.** Frequency-magnitude distribution for (a) the broader Kanto area (Figure 3 outer box) and (b) the area of completeness (Figure 3, inner box). Rates for $M < 6.7$ are from the instrumental catalog (1924–2003). Rates for $6.7 \leq M \leq 7.4$, are from the extended catalog (1649–2003) with error bars representing the 95% confidence interval. Rates for Taisho-type and Genroku-type events are from paleoseismic data [*Stein et al.*, 2006; *Shishikura*, 2003]. The solid line is the least squares truncated G-R *Kagan* [1991] equation. The dashed line shows the G-R equation without truncation.

[24] Extending the parameterized *Kagan* [1991] equation without truncation (dashed lines in Figure 4) would predict higher rates for the largest shocks. This would be appropriate if the catalog undersamples the largest earthquakes because only those events that uplift marine terraces or leave tsunami deposits are recognized.

### 4.3. Catalog Moment

[25] We next calculate the total scalar moment for the catalog period under the assumption that the intensity-based catalog is complete for large events that dominate seismic moment. *Utsu* [1982b] and *Katsumata* [1996] found that the difference between $M_{JMA}$ and $M_w$ is generally not significant for shallow $M = 4.5$–$7.5$ earthquakes from the 1926–1994 period analyzed; the average difference is less than 0.1 magnitude units. Recent notable exceptions, such as the 2000 Tottori earthquake ($M_{JMA} = 7.3$, $M_w = 6.6$ [*Furumura et al.*, 2003]), demonstrate that large discrepancies do rarely occur. However, since we model all earthquakes with depths less than 30 km and much greater sources of uncertainty exist in the intensity-based models, $M_{JMA}$ is simply substituted for $M_w$ in the *Hanks and Kanamori* [1979] equation, $M_o = 10^{1.5(M_w+10.7)}$ dyn cm.

[26] A basic calculation of the catalog moment could be made using the magnitude at the intensity center for each earthquake, $2.7 \times 10^{28}$ dyn cm. However, such an approach fails to incorporate the evident uncertainties in magnitude for each earthquake shown in Figure 2 and Appendix A. Magnitude estimates from the intensity-based models contain independent magnitude uncertainty; *Bakun* [2005] determined that intensity-based magnitude contours for test earthquakes from the instrumental catalog were accurate within $\pm 0.25$ $M_{JMA}$ units at the 67% confidence level at the epicenter location. Estimates of magnitude also contain covariant uncertainty with location since the location of the epicenter will determine the magnitude needed to fit the intensity data.

[27] To propagate these compound uncertainties, we use a Monte Carlo simulation to generate 100,000 realizations of the summed moment for the historical intensity-based catalog. In each Monte Carlo iteration, a probabilistic weighting algorithm chooses one possible realization of location and magnitude for each catalog earthquake. The algorithm is designed so that, for any earthquake, the likelihood that the earthquake will be placed in a particular location corresponds to the confidence level for that location as defined by model

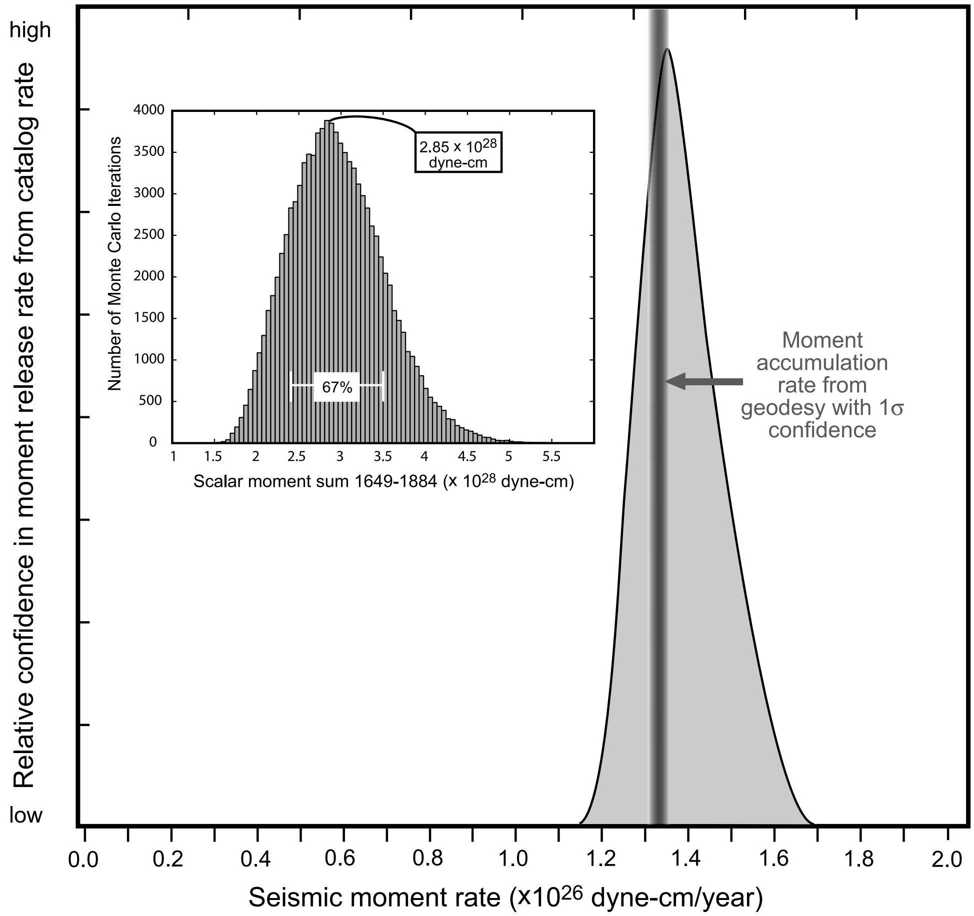


**Figure 5.** Monte Carlo statistics for catalog scalar moment and comparison with moment accumulation rates from geodesy. Light curve shows the relative confidence for the 1649–2003 moment rate. The dark band is the moment accumulation rate estimated from geodesy (Nishimura et al., submitted manuscript, 2005) with $1\sigma$ uncertainty. Inset gives Monte Carlo statistics for total scalar moment for the 1649–1884 catalog.

RMS[$M_{jma}$]. Thus 95% of the time, an outcome location is picked within the 95% confidence contour; 67% of the time, the earthquake is located within the 67% confidence contour. Ten confidence ranges between 50% and 95%, from Table 5b of *Bakun and Wentworth* [1997], are used to constrain the location. The outcome magnitude for each event is derived from the corresponding model magnitude for the outcome location, but is also subsequently modified according to independent magnitude uncertainties. The independent uncertainty, $\pm 0.25$ $M_{JMA}$, is propagated using a random Gaussian number generator so that the final output magnitude has a Gaussian probability distribution centered on the model magnitude.

[28] By the end of one Monte Carlo iteration, the probabilistic outcome algorithm has created one realization of the entire catalog with discrete magnitudes for every event. After creating 100,000 of these hypothetical catalogs, the scalar moment sum for each catalog, $M_{o,n}$, is calculated. More probable results for the moment sum occur more often in the total set of iterations. Therefore the statistical distribution of all 100,000 $M_{o,n}$ defines the best estimate and uncertainties of scalar moment represented in the catalog.

[29] The Monte Carlo results are shown in Figure 5 inset. The distribution is slightly skewed, in part due to the logarithmic relationship between moment and magnitude which will cause a relatively centered distribution in magnitude to appear skewed when expressed as moment. A peak is centered near $3 \times 10^{28}$ dyn cm, but a thin tail extends to over $5.5 \times 10^{28}$ dyn cm. The mean ($2.95 \times 10^{28}$) and standard deviation ($0.56 \times 10^{28}$) are sensitive to extreme values and are not ideally representative. When the histogram is grouped into 80 bins, the peak occurs at $2.85 \times 10^{28}$ dyn cm; this value is the most frequent outcome in the set of iterations, and thus the highest-confidence estimate of catalog scalar moment. Sixty-seven percent of the outcomes centered on this peak range from 2.41 to $3.50 \times 10^{28}$ dyn cm; the 95% confidence range is 2.00 to $4.16 \times 10^{28}$ dyn cm.

[30] The scalar moment sum is next corrected for the missing $M \leq 6.7$ shocks. Because the intensity-based catalog is not complete for earthquakes $M < 6.7$, the moment contribution from these events is not included in the above calculation. This missing moment can be approximated, however, by translating the Gutenberg-Richter relation from a magnitude-frequency relation to a moment-frequency relation and integrating this new function from $-\infty$ to $M_o(M = 6.7)$ following *Andrews and Schwerer* [2000]. Using the Gutenberg-Richter equation for the area of completeness, the moment contribution from events $M < 6.7$ is calculated as $4.76 \times 10^{27}$ dyn cm for the 235-year period (1649–1884), or 16% of the total moment. Therefore the best estimate of total scalar moment for 1649–1884 is 3.33 (−0.4, + 0.7) ×

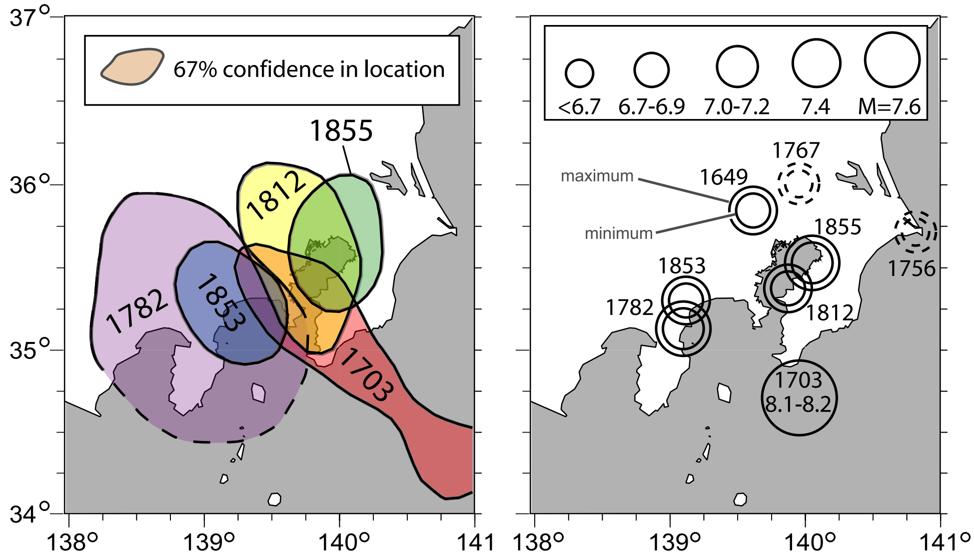


**Figure 6.** Uncertainties associated with the largest earthquakes in the 1649–1884 catalog. Colored areas on left are 67% location confidence contours using *Bakun* [2005] intensity-attenuation models (dashed where constrained by judgment). Concentric circles on right are 1$\sigma$ confidence range in magnitude (dashed where highly uncertain).

$10^{28}$ dyn cm (1$\sigma$). Incorporating the moment contribution from the 1885–1922 *Utsu* [1982a] catalog and the 1923–2003 instrumental catalog (inner box, Figure 3) yields an average moment rate of 1.35 (−0.11, +0.20) × $10^{26}$ dyn cm yr$^{-1}$(1$\sigma$) from 1649 to 2003 (Figure 5).

[31] The moment rate and uncertainty is dominated by the largest event in the historical catalog, the 1703 Genroku earthquake ($M_o$ = 1.3–2.7 × $10^{28}$ dyn cm). The *Shishikura and Toda* [2003] model for Genroku is used in place of the intensity-based model (Figure 2b) for the Monte Carlo simulation because it incorporates the entire suite of available data including tsunami runup heights and surface fault displacement. Genroku contributes 75–95% of the 1649–1884 moment rate and ≤ 56% of the long-term 1649–2003 moment rate; the 1923 great Kanto earthquake ($M$ = 7.9) represents another 20% of the moment. The second largest event in the intensity-based catalog, the 1855 Ansei-Edo earthquake ($M$ = 7.1–7.6), accounts for only ~3% of the long-term moment rate. However, this and several other large events in the catalog (Figure 6) account for more than 20% of the total uncertainty in catalog moment and so are important to consider in the moment estimation.

## 5. Discussion

### 5.1. Comparison With the *Usami* [2003] Catalog and Isoseismal Methods

[32] The catalog proposed in this study differs significantly from that of *Usami* [2003] (Figure 1). Magnitudes for most earthquakes calculated here are greater than the *Usami* [2003] magnitudes; the mean increase is 0.3 $M_{JMA}$ units. In addition, inferred epicenters from this study are less tightly clustered around Tokyo and suggest a more dispersed region of seismicity, consistent with the instrumental catalog (Figure 3). Perhaps the more important difference, though, is that this catalog quantitatively describes the significant uncertainty and covariance between location and magnitude which can be extremely important in risk analyses. The uncertainties conveyed here have meaning both for individual earthquakes and the collective catalog; Figure 6 shows combined uncertainties for the largest, most important events in the catalog.

### 5.2. Model Simplifications and Possible Sources of Error

[33] The *Bakun and Wentworth* [1997] method makes simplifications in the intensity-attenuation models so that predicted intensity observations are a function of only two parameters: magnitude and distance from a point source. Simplifying a finite fault to a point source may introduce some location error as the location of the intensity center corresponds to the moment centroid [*Bakun*, 2005] rather than the epicenter. If the point source approximation results in magnitude error, the Bakun-Wentworth method should produce erroneously high magnitudes for large events. This is because observations located near the edge of a large rupture plane, but far from a theoretical point source, would produce unexpectedly high intensities at their radial distance from the intensity center. However, because the method yields the correct magnitude for the great 1923 Kanto $M$ = 7.9 earthquake and other large test earthquakes [*Bakun*, 2005], magnitude overestimation is probably not a significant problem.

[34] The *Bakun* [2005] equations also simplify energy radiation and attenuation as isotropic effects and so neglect the anisotropic nature of the structures on which these earthquakes occur. For example, a subducting plate that acts as a waveguide will alter the distribution of intensities and cause error in magnitude and location estimates. In a regional sense, uncertainty introduced by these effects should be represented on average by the location confidence contours and magnitude uncertainty developed by *Bakun* [2005]. However, corrections can be applied locally, as discussed in the following section, in cases where a systematic bias is identified.

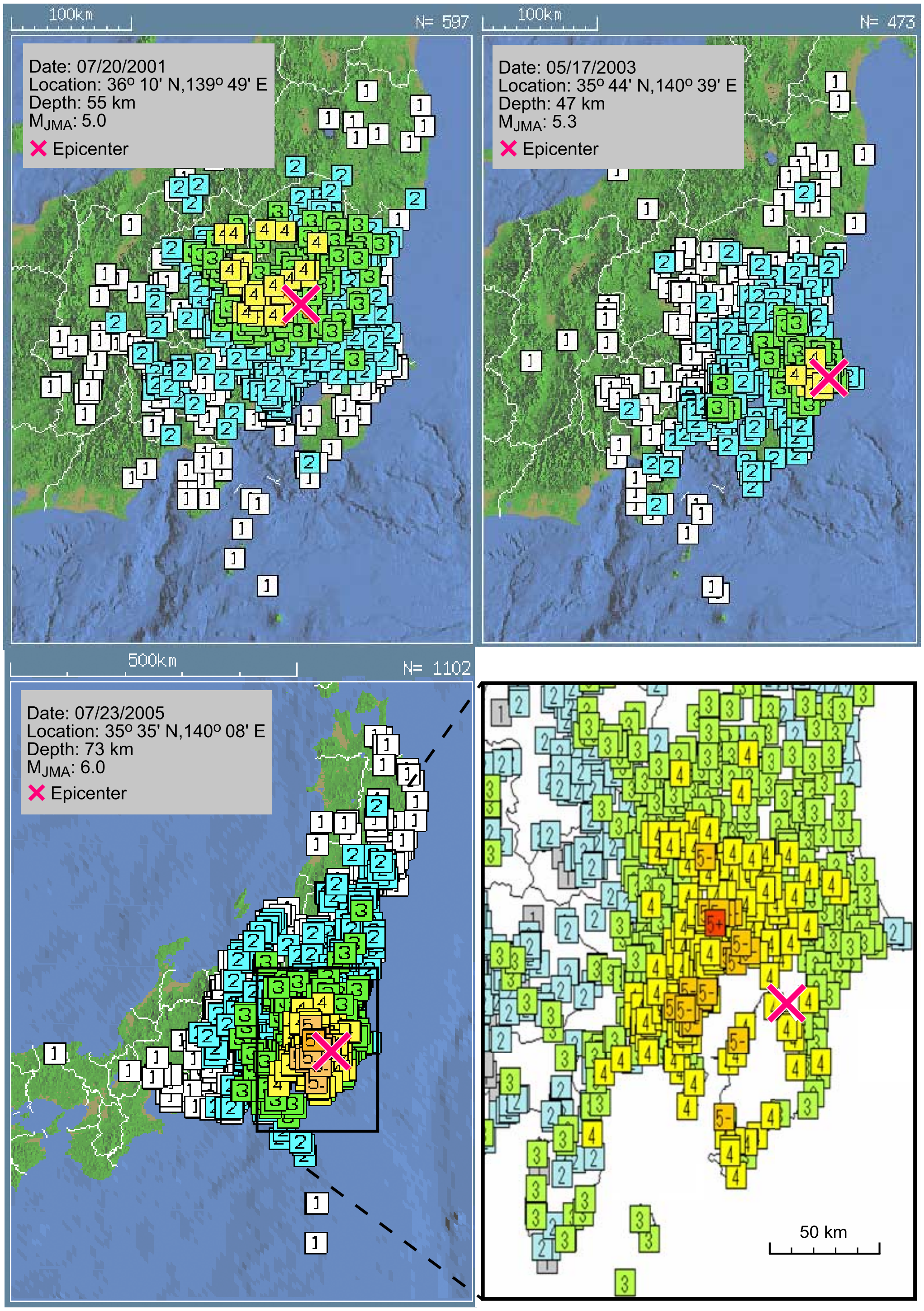


**Figure 7.** Three examples of modern earthquakes showing systematic bias between the location of the highest intensities and the precisely located epicenter (JMA).

## 5.3. Intensity Center Versus Epicenter Bias

[35] The intensity centers locations determined in this study are the best approximation based on the historical intensity data and the calibrated *Bakun* [2005] attenuation models. However, modern Kanto earthquakes indicate that the highest intensities are typically registered ~25 km northwest of the epicenter for earthquakes around Tokyo Bay and the Boso Peninsula (Figure 7) (JMA, 2005, http://www.jma.go.jp). One physical explanation for this bias is that waves traveling north down the Philippine Sea plate slab or west down the Pacific plate slab propagate with lower attenuation and thus shift the locus of strongest shaking [*Nakamura et al.*, 1994]. Second, shallow alluvial deposits extending along the western margin of Tokyo Bay and northwest of Tokyo [*Geological Survey of Japan*, 2003] amplify shaking, and so all sources produce higher intensity

**Table 3.** Statistics of Location Bias for Intensity Observations From Recent Earthquakes

| Date | Latitude | Longitude | Depth, km | JMA Magnitude | Intensity Bias | |
|---|---|---|---|---|---|---|
| | | | | | West, km | North, km |
| 2/16/2005 | 36.03 | 139.90 | 45 | 5.4 | −15 | 5 |
| 7/10/2004 | 36.08 | 139.88 | 48 | 4.7 | −5 | 20 |
| 5/31/2001 | 36.18 | 139.80 | 56 | 4.7 | 0 | 15 |
| 7/15/1999 | 35.93 | 140.43 | 50 | 5.0 | 10 | 15 |
| 4/8/2003 | 36.07 | 139.92 | 47 | 4.6 | 15 | 20 |
| 5/12/2003 | 35.88 | 140.07 | 50 | 4.6 | 15 | 15 |
| 10/15/2003 | 35.62 | 140.05 | 74 | 5.1 | 15 | −5 |
| 2/23/2005 | 36.10 | 139.85 | 50 | 4.4 | 15 | 15 |
| 6/3/2000 | 35.68 | 140.75 | 48 | 6.0 | 20 | 0 |
| 7/20/2001 | 36.17 | 139.82 | 55 | 5.0 | 20 | 20 |
| 5/17/2003 | 35.73 | 140.65 | 47 | 5.3 | 20 | 10 |
| 2/4/2004 | 36.00 | 140.08 | 65 | 4.2 | 20 | 25 |
| 4/11/2005 | 35.57 | 140.18 | 73 | 4.4 | 20 | 10 |
| 4/11/2005 | 35.73 | 140.62 | 52 | 6.1 | 20 | 15 |
| 11/8/1998 | 35.63 | 140.03 | 80 | 4.7 | 25 | 15 |
| 9/20/2003 | 35.22 | 140.30 | 70 | 5.8 | 20 | 20 |
| 2/8/2005 | 36.13 | 140.08 | 67 | 4.8 | 25 | 15 |
| 7/23/2005 | 35.01 | 139.96 | 74 | 6.1 | 25 | 5 |
| 8/18/2003 | 35.80 | 140.12 | 69 | 4.8 | 30 | 15 |
| 4/17/2005 | 35.15 | 139.97 | 69 | 4.4 | 30 | 15 |
| 9/13/1999 | 35.60 | 140.17 | 76 | 5.1 | 35 | 20 |

observations at these sites [see *Stein et al.*, 2006, Figure 7]. Further, for historical intensity data sets, there is a sampling bias because of the concentration of observations at population centers near Tokyo and Yokohama.

[36] To quantify the intensity center-epicenter shift, we use 20 recent earthquakes from the Kanto area, for which dense intensity observations and precisely located epicenters are available. Measuring the distance from the epicenter to the center of the highest intensities for each earthquake, we find that intensity observations are biased to the west by 20.5 ± 11.5 km and to the north by 16.0 km ± 8.9 ($1\sigma$) (Table 3). Since it is likely that this bias influences the location of intensity data for the historical earthquakes, inferred epicenters for the historical catalog are located 20.5 km to the east and 16.0 km south of the original intensity centers (Figure 1b). Magnitude estimates are also likely to be influenced by local amplification, especially when intensity data are very sparse (e.g., 1767), but because this effect cannot be quantified for each datum location, no magnitude correction is applied. This analysis therefore does not change the moment calculation or the magnitude-frequency distribution. Similar location biases may exist in other regions of Japan, but no offset is applied to the four earthquakes near the Izu Peninsula because recent earthquakes in this region do not exhibit a significant systematic bias.

## 5.4. Gutenberg-Richter Relation at Large Magnitudes

[37] The truncated Gutenberg-Richter relation determined here (Figure 4b) is appropriate if the intensity-based catalog is complete for large events. An alternative possibility is that the distribution is not truncated, or at least is not truncated at $M = 8.4$, in which case the catalog would be missing more than half of the expected $M \sim 8$ shocks (see dashed versus solid black lines in Figure 4). If some of the largest shocks were located far offshore, they may have escaped detection. There is, for example, an unlocatable 1677 shock [*Usami*, 2003] which triggered a tsunami and caused 246 drownings on the Boso peninsula, and so could be an $M \sim 8$ event far offshore [*Earthquake Research Committee*, 1998]. Additionally, there may be great offshore earthquakes in this area with interevent times longer than the historical record and for which a paleoseismic proxy such as marine terraces has not been identified. However, the smaller box in particular does not extend far offshore, and so should not suffer from this problem. Also, the $M_{\max}$ parameter is not simply defined by the largest event in the catalog ($M = 8.2$) but by gradual tapering throughout the higher magnitude range. Thus it seems more likely that the distribution is, in fact, truncated.

[38] The parameterized *Kagan* [1991] equation fits the Kanto data continuously for $4.5 \leq M \leq 8.2$. Even the largest earthquakes in the catalog conform to this truncated Gutenberg-Richter distribution, rather than what is sometimes termed a characteristic earthquake distribution [*Wesnousky*, 1994], which would predict much higher rates for the largest events (see Figure 4b inset). The Kanto catalog stands in contrast to results from *Wesnousky* [1994], who found that most faults in California exhibit a characteristic earthquake distribution when interevent times for the largest events are considered. However, interevent times from *Wesnousky* [1994] were based on very limited historical and paleoseismic data, whereas interevent times used in this study are based on a ~7000 year record of 17 great earthquakes.

## 5.5. Moment Balance With Current Strain Rates

[39] The 1649–2003 extended catalog can be used to compare the long-term rate of seismic moment release with current moment accumulation rates inferred from geodetically measured strain. The subduction boundary of the Philippine Sea plate is strongly coupled on the basis of geodesy [*Sagiya*, 2004; T. Nishimura et al., Crustal block kinematics and seismic potential of the northernmost Philippine Sea plate and Izu microplate, central Japan, inferred from GPS and leveling data, submitted to *Journal of Geophysical Research*, 2005, hereinafter referred to as Nishimura et al., submitted manuscript, 2005] except for

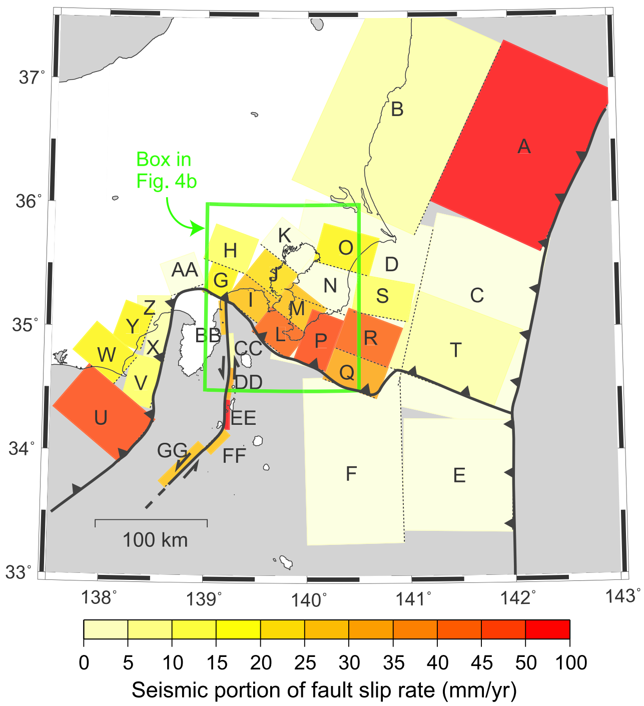


**Figure 8.** Nishimura et al. (submitted manuscript, 2005) slip deficit model from recent geodetic data. Solid lines represent surface traces of the plate boundaries. More positive values reflect higher moment accumulation rates. The green box shows the area of completeness for the historical catalog.

the east of Boso transient slip zone, which lies at the edge of the catalog area. Thus, over a sufficiently long period of time, interseismic elastic strain accumulation should be balanced by strain release associated with seismic slip. Marine terrace uplift, such as that along the Boso coast, results from repeated earthquake slip on the subduction interface, and does not represent permanent unrecoverable strain [*Thatcher and Rundle*, 1979].

[40] Interseismic elastic strain in a subduction zone can be modeled as back slip in the opposite direction of plate motion; this back slip can be regarded as a slip deficit that is recovered during earthquakes [*Savage*, 1983]. Nishimura et al. (submitted manuscript, 2005) inverted GPS and leveling data to calculate interseismic slip deficit rates in the Kanto area. They found that strain accumulation in southern Kanto can be fully satisfied by coupled slip on the Philippine Sea plate subduction boundary and the Izu-microplate strike-slip zone (Figure 8). As far as can be discerned, coupling along these main structures drives the observed seismicity in southern Kanto.

[41] In order to compare these results with catalog moment release, the slip deficit rates are related to the rate of seismic moment accumulation according to the dislocation theory of faulting [*Burridge and Knopoff*, 1964], $\langle u \rangle = Mo/\mu A$, where $\langle u \rangle$ is the average slip over the fault surface, $\mu$ is crustal rigidity (taken as $3.8 \times 10^{11}$ dyn cm$^{-2}$ for regional subduction events [*Sato et al.*, 1998]), and $A$ is the area of fault slip. Table 4 shows conversions of Nishimura et al. (submitted manuscript, 2005) slip deficit rates to moment accumulation rates. Uncertainties associated with the moment accumulation rate are mostly due to limited offshore stations and are listed in Table 4.

[42] Using the portion of Nishimura et al. (submitted manuscript, 2005) sources within the area of catalog completeness (Figure 8), the moment accumulation rate is $1.33 \pm 0.10 \times 10^{26}$ dyn cm yr$^{-1}$. This rate is in substantial agreement with the with long-term seismic moment rate (Figure 5), $1.35 \times 10^{26}$ dyn cm yr$^{-1}$, the vast majority of which is associated with the 1703 and 1923 events. Assuming aseismic slip is negligible [*Sagiya*, 2004], this agreement implies that regional moment accumulation and moment release are likely balanced over the time span of the catalog. Taken at face value, this result suggests that the 354-year catalog is representative of long-term seismic processes in the Kanto area. Alternatively, if we assume the catalog is complete and representative, the balance implies that the current rate of strain accumulation typifies the long-term strain rate.

[43] There is, however, an important caveat to the apparent moment accumulation and release balance. Because catalog moment calculations include the entire moment contribution from the 1703 Genroku shock, an earthquake

**Table 4.** Moment Accumulation Rates Calculated From the Nishimura et al. (submitted manuscript, 2005) Slip Deficit Model[a]

| Source | Length, km | Width, km | Included, % | Slip Deficit Rate, mm/yr | Formal Uncertainty, mm/yr | Resolution,% | Moment Rate, dyn cm/yr | Uncertainty, dyn cm/yr |
|---|---|---|---|---|---|---|---|---|
| G | 24 | 30 | 100 | 16 | 0.4 | 100 | 4.38E + 24 | 1.09E + 23 |
| H | 40 | 35 | 100 | 12 | 0.8 | 100 | 6.38E + 24 | 4.26E + 23 |
| I | 37 | 30 | 100 | 28 | 0.5 | 100 | 1.18E + 25 | 2.11E + 23 |
| J | 37 | 30 | 100 | 22 | 0.9 | 100 | 9.28E + 24 | 3.80E + 23 |
| K | 43 | 33 | 100 | 4 | 0.9 | 100 | 2.16E + 24 | 4.85E + 23 |
| L | 40 | 30 | 100 | 40 | 0.8 | 100 | 1.82E + 25 | 3.65E + 23 |
| M | 40 | 30 | 100 | 26 | 1.0 | 100 | 1.19E + 25 | 4.56E + 23 |
| N | 51 | 35 | 100 | 3 | 0.9 | 100 | 2.03E + 24 | 6.10E + 23 |
| O | 51 | 35 | 75 | 18 | 0.8 | 100 | 9.16E + 24 | 4.07E + 23 |
| P | 30 | 50 | 100 | 48 | 0.7 | 50 | 2.74E + 25 | 3.99E + 23 |
| Q | 51 | 30 | 60 | 30 | 1.0 | 1 | 1.05E + 25 | 3.49E + 23 |
| R | 51 | 38 | 30 | 41 | 0.8 | 35 | 9.06E + 24 | 1.77E + 23 |
| S | 51 | 35 | 10 | 10 | 0.8 | 32 | 6.78E + 23 | 5.43E + 22 |
| BB | 30 | 14.9 | 100 | 28 | 0.7 | 100 | 4.76E + 24 | 1.19E + 23 |
| CC | 30.5 | 14.9 | 100 | 9 | 1.5 | 100 | 1.55E + 24 | 2.59E + 23 |
| DD | 28 | 14.9 | 75 | 31 | 1.6 | 100 | 3.69E + 24 | 1.90E + 23 |

[a]Read 4.38E + 24 as $4.38 \times 10^{24}$.

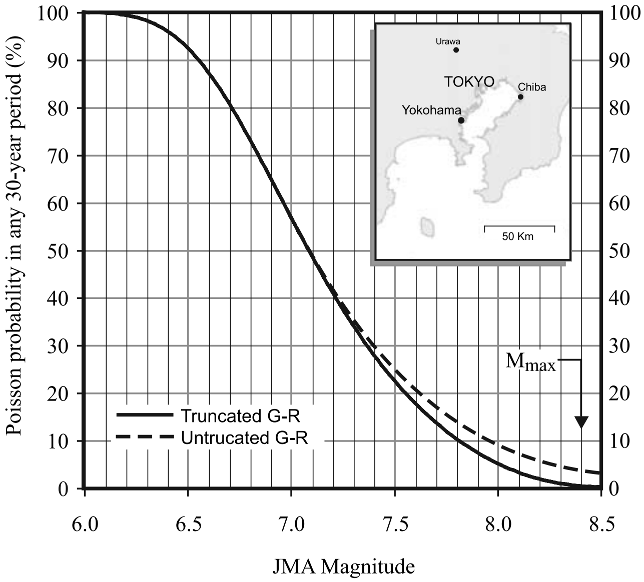


**Figure 9.** Thirty-year time-averaged probability of earthquakes. Poisson probabilities reflect likelihood that at least one earthquake magnitude $M$ or larger will occur during any 30-year period within the area shown in the inset map. The solid line and dashed line are based on the truncated and untruncated Gutenberg-Richter equation, respectively.

with an interevent time six times longer than the period of the catalog (~2200 years [*Shishikura*, 2003]), one might expect the A.D. 1649–2003 moment rate to exceed strain rate predictions. If instead, only one sixth of the Genroku moment is included, moment rates would underestimate the strain predictions by roughly 50%. On the other hand, we exclude the potential moment contribution from the 1677 event which may be quite large.

### 5.6. Earthquake Hazard Probabilities

[44] The Gutenberg-Richter equation for the area of completeness defines a Poisson time-averaged probability for earthquakes, $1 - e^{-\lambda t}$, during a time interval t, where $\lambda$ is the rate of earthquakes magnitude $M$ or greater (Figure 9). During an average 30-year period, there is a 57% probability of at least one $M \geq 7.0$ shock occurring within the catalog area. A similar probability of 53% is implied by the instrumental catalog in which there are two $M \geq 7.0$ earthquakes excluding the 1923 Kanto earthquakes and its aftershocks. If such a large earthquake occurs offshore near the southern boundary of the catalog area, Tokyo may experience only minor damage, but an $M = 7$ event in close proximity to the metropolitan area would likely cause significant damage.

[45] Probabilities for $M > 7.5$ shocks differ depending on whether the Gutenberg-Richter relation is truncated. The probability for a repeated Taisho-type ($M = 7.9$) event is just 7% according to the truncated Gutenberg-Richter equation; without truncation this probability rises to 11%. The time-dependent probability for this event is likely to be even lower due to the rather recent occurrence of the great Kanto earthquake in 1923 in comparison to its mean ~400-year interevent time. If the Gutenberg-Richter relation continues without truncation, there is a 3% probability of an event $M > 8.5$. Although the catalog suggests that such large shocks do not occur, this small probability is an important consequence if the largest shocks in the catalog are undersampled.

## 6. Conclusions

[46] This study has produced a new historical catalog using intensity assignments from *Usami* [1994] and the calibrated *Bakun* [2005] intensity attenuation models for Japan. While it is not possible to conclude that the precise source parameters determined in this study are more accurate than those found by *Usami* [2003], the intensity-attenuation relations used here are calibrated to modern Japanese earthquakes and have been shown to be highly accurate for modern test earthquakes [*Bakun*, 2005]. The catalog is likely complete for shocks $M \geq 6.7$ and provides meaningful estimates of magnitude and location uncertainties, which have not been rigorously quantified in previous studies but which are often very significant. When merged with the 80-year instrumental record, the intensity-based catalog represents the past 350 year of damaging earthquakes near Tokyo.

[47] The rich ~7000-year paleoseismic record permits one to define a truncated Gutenberg-Richter distribution that is consistent over a very wide magnitude range. The rate of moment release for the 1649–2003 extended catalog contains significant uncertainty (−8%, +15%) but is approximately in balance with predicted moment accumulation rates determined from modern geodetic studies. This likely balance and the natural frequency-magnitude distribution suggest that the 1649–2003 catalog is roughly representative of the long-term seismic process near Tokyo, and is thus representative of the style and spatial distribution of seismic sources.

[48] The frequency-magnitude distribution defined in this study can therefore be used to develop earthquake probabilities for future seismicity in the area. The time-averaged 30-year probability for earthquakes $M > 7.0$ is 57%. The time-averaged probability for shocks on the scale of the great 1923 Kanto earthquake is 7–11%, though the time-dependent probability must be much lower. It remains possible, but unlikely, that still larger shocks are missing from the catalog, and that earthquakes larger than the 1703 Genroku earthquake $M = 8.2$ may strike the Tokyo area.

## Appendix A

[49] Intensity-based models for 15 earthquakes which occurred between 1649 and 1884 are developed using the *Bakun and Wentworth* [1997] algorithm and *Bakun* [2005] intensity attenuation relationships. Earthquakes for which there are fewer than two damage-based intensity observations are not included in this study. Resulting location and magnitude confidence plots for these earthquakes are provided in Figure A1 and show the epicenter determined by *Usami* [2003] for comparison. User-specified modeling parameters for each earthquake are listed in Table 2.

[50] For many earthquakes, our estimated magnitude and location are in relative agreement with those inferred by *Usami* [2003] (e.g. 1843, 1853, and 1859). In some cases, however, we find a significantly different location or

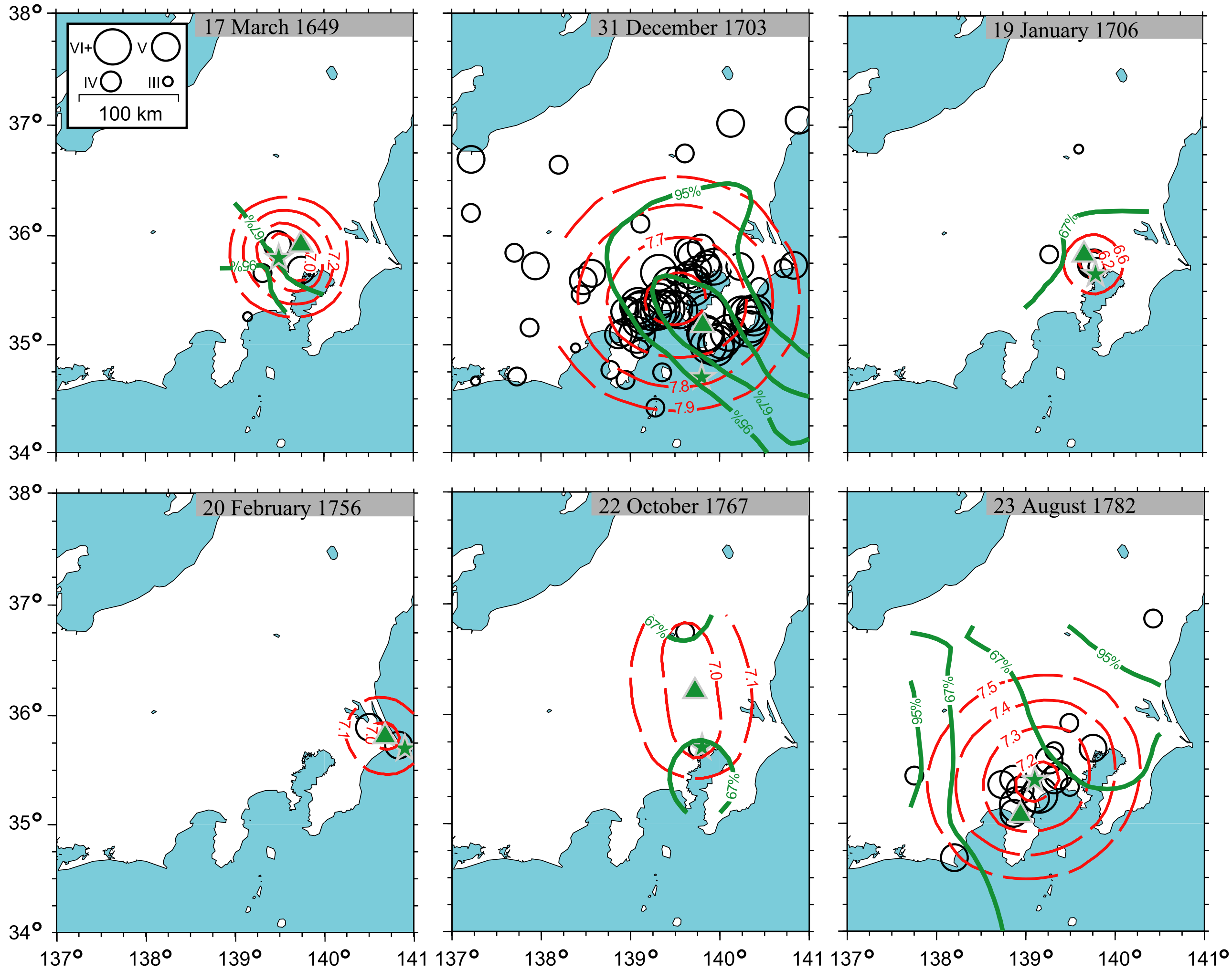


**Figure A1.** All 15 earthquake models in the intensity-based catalog. Dashed contours are $M_{jma}$, and solid contours are the 67% and 95% location confidence contours where shown. The triangle is the location of the intensity. The star is the location of the *Usami* [2003] epicenter.

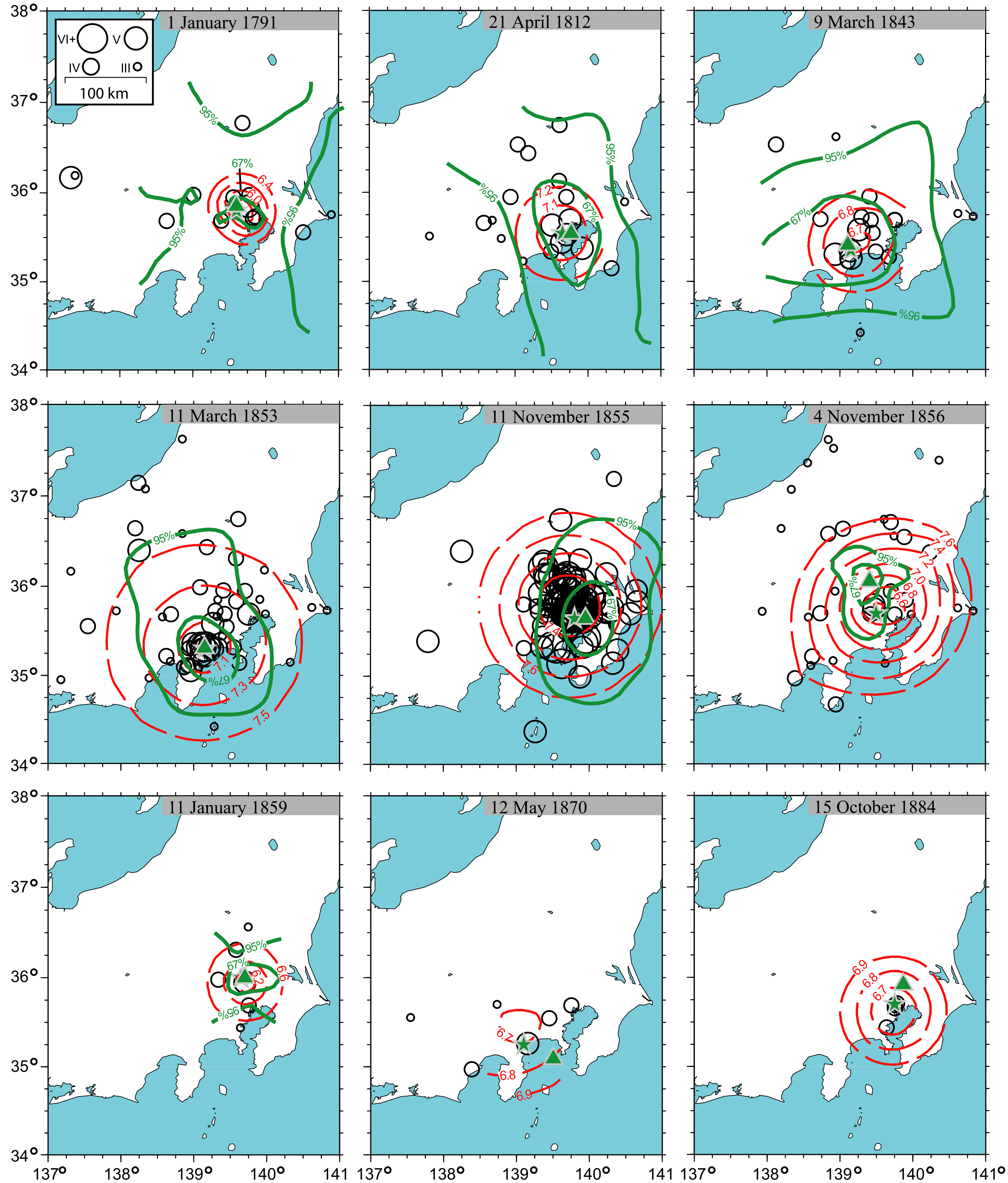


**Figure A1.** (continued)

magnitude (e.g. 1703, 1812, and 1856). Unfortunately, two earthquakes in 1756 and 1767 have insufficient intensity data to be adequately constrained by these methods. Magnitude and location results from this catalog are incorporated with modern instrumental seismic data to assess long-term seismic processes near Tokyo and the potential for future hazards.

[51] **Acknowledgments.** This work was carried out at the U.S. Geological Survey as part of a broader project to assess Tokyo's seismic hazard. Swiss Re has provided funding for our project and we are grateful

for their support. We thank Bill Bakun of the U.S. Geological Survey for sharing executable programs for his model algorithms and providing valuable suggestions throughout the course of this study. Serkan Bozkurt of the USGS and Shinji Toda of the Geological Survey of Japan have also supplied important data. Translations of some Japanese references have been provided by Ayako Kameda.

## References

Andrews, D. J., and E. Schwerer (2000), Probability of rupture of multiple fault segments, *Bull. Seismol. Soc. Am.*, *90*, 1498–1506.

Bakun, W. H. (2005), Magnitude and location of historical earthquakes in Japan and implications for the 1855 Ansei Edo earthquake, *J. Geophys. Res.*, *110*, B02304, doi:10.1029/2004JB003329.

Bakun, W. H., and C. M. Wentworth (1997), Estimating earthquake location and magnitude from seismic intensity data, *Bull. Seismol. Soc. Am.*, *87*, 1502–1521, (Erratum, *Bull. Seismol. Soc. Am.*, *89*, 577, 1999.)

Burridge, R., and L. Knopoff (1964), Body force equivalents for seismic dislocations, *Bull. Seismol. Soc. Am.*, *54*, 1875–1888.

Earthquake Research Committee (1998), Seismic activity in Japan, report, 222 pp., Headquarters Earthquake Res. Promotion, Tokyo.

Furumura, T., B. L. N. Kennett, and K. Koketsu (2003), Visualization of 3D wave propagation from the 2000 Tottori-ken Seibu, Japan, earthquake: Observation and numerical simulation, *Bull. Seismol. Soc. Am.*, *93*, 870–881.

Geological Survey of Japan (2003), Geological map of Japan, in *Geological Survey of Japan AIST* [CD-ROM], 3rd ed., scale 1:1,000,000, *Adv. Ind. Sci. and Technol.*, Tsukuba, Japan.

Gutenberg, B., and C. F. Richter (1944), Frequency of earthquakes in California, *Bull. Seismol. Soc. Am.*, *34*, 185–188.

Hamada, N., Y. Kazumitsu, M. Nishwaki, and M. Abe (2001), A comprehensive study of aftershocks of the 1923 Kanto earthquake (in Japanese), *Bull. Seismol. Soc. Jpn.*, *54*, 251–265.

Hanks, T. C., and H. Kanamori (1979), A moment magnitude scale, *J. Geophys. Res.*, *84*, 2348–2350.

Imamura, A. (1924), Preliminary note on the great earthquake of S.E. Japan on Sept. 1, 1923, *Seismol. Notes Imp. Earthquake Invest. Comm.*, *6*, 136–149.

Ishida, M. (1992), Geometry and relative motion of the Philippine Sea plate and the Pacific plate beneath the Kanto-Tokai District, Japan, *J. Geophys. Res.*, *97*, 489–513.

Japan Meteorological Agency (JMA) (2004), *Annual Seismological Bulletin* [CD-ROM], Tokyo.

Kagan, Y. Y. (1991), Seismic moment distribution, *Geophys. J. Int.*, *106*, 123–134.

Katsumata, A. (1996), Comparison of magnitudes estimated by the Japan Meteorological Agency with moment magnitudes for intermediate and deep earthquakes, *Bull. Seismol. Soc. Am.*, *86*, 832–842.

Matsuda, T., Y. Ota, M. Ando, and N. Yonekura (1978), Fault mechanism and recurrence time of major earthquakes in Southern Kanto district, Japan, as deduced from coastal terrace data, *Geol. Soc. Am. Bull.*, *89*, 1610–1628.

Nakamura, R., K. Shimazaki, and T. Hashida (1994), 3-D attenuation structure beneath the Japanese Islands by tomographic inversion of seismic intensity data and predicting JMA intensity distribution in a broad area (in Japanese), *J. Seismol. Soc. Jpn.*, *47*, 21–32.

Nyst, M., T. Nishimura, F. F. Pollitz, and W. Thatcher (2006), The 1923 Kanto earthquake reevaluated using a newly augmented geodetic data set, *J. Geophys. Res.*, *111*, B11306, doi:10.1029/2005JB003628.

Ozawa, S., S. Miyazaki, Y. Hatanaka, T. Imakiire, M. Kaidzu, and M. Murakami (2003), Characteristic silent earthquakes in the eastern part of the Boso peninsula, central Japan, *Geophys. Res. Lett.*, *30*(6), 1283, doi:10.1029/2002GL016665.

Sagiya, T. (2004), Interplate coupling in the Kanto district, central Japan, and the Boso Peninsula silent earthquake in May 1996, *Pure Appl. Geophys.*, *161*, 2327–2342.

Sato, T., R. W. Graves, P. G. Somerville, and S. Kataoka (1998), Estimates of regional and local strong motions during the great 1923 Kanto, Japan, earthquake (Ms 8.2), *Bull. Seismol. Soc. Am.*, *88*, 206–227.

Savage, J. C. (1983), A dislocation model of strain accumulation and release at a subduction zone, *J. Geophys. Res.*, *88*, 4984–4996.

Shishikura, M. (2003), Cycle of interplate earthquakes along the Sagami Trough deduced from tectonic geomorphology, *Bull. Earthquake Res. Inst. Univ. Tokyo*, *78*, 245–254.

Shishikura, M., and S. Toda (2003), Recurrence of characteristic Kanto earthquakes and unusual 1703 type earthquakes inferred from emerged shoreline topography, *Eos Trans. AGU*, *84*(46), Fall Meet. Suppl., Abstract S51G-08.

Stein, R. S., S. Toda, T. Parsons, and E. Grunewald (2006), A new probabilistic seismic hazard assessment for greater Tokyo, *Proc. R. Soc. London, Ser. A*, *364*, doi:10.1098/rsta.2006.1808.

Thatcher, W., and J. B. Rundle (1979), A model for the earthquake cycle in underthrust zones, *J. Geophys. Res.*, *84*, 5540–5556.

Usami, T. (1994), Seismic intensity maps and isoseismal maps of historical earthquakes of Japan (in Japanese), Jpn. Electr. Assoc., Tokyo.

Usami, T. (2003), *Materials for Comprehensive List of Destructive Earthquakes in Japan* (in Japanese), 605 pp., Univ. of Tokyo Press, Tokyo.

Utsu, T. (1979), Seismicity of Japan from 1885 through 1925—A new catalog of earthquakes of $M \geq 6$ felt in Japan and smaller earthquakes which caused damage in Japan (in Japanese), *Bull. Earthquake Res. Inst. Univ. Tokyo*, *54*, 253–308.

Utsu, T. (1982a), Catalog of large earthquakes in the region of Japan from 1885 through 1980 (in Japanese), *Bull. Earthquake Res. Inst. Univ. Tokyo*, *57*, 401–463.

Utsu, T. (1982b), Relationships between earthquake magnitude scales (in Japanese), *Bull. Earthquake Res. Inst. Univ. Tokyo*, *57*, 465–497.

Wesnousky, S. (1994), G-R or characteristic earthquake distribution: Which is it?, *Bull. Seismol. Soc. Am.*, *84*, 1940–1959.

Wyss, M., and S. Wiemer (1997), Two current seismic quiescences within 40 km of Tokyo, *Geophys. J. Int.*, *128*, 459–473.

E. D. Grunewald, Department of Geophysics, Stanford University, 397 Panama Mall, Mitchell Building 360, Stanford, CA 94305, USA. (elliotg@pangea.stanford.edu)

R. S. Stein, U.S. Geological Survey, 345 Middlefield Road, MS 977, Menlo Park, CA 94025, USA.